


Evaluation of compositing algorithms from the regular and non-regular intervals using MODIS daily images in the Amazon region with a high percentage of cloud cover

*Cristiane Batista Salgado*¹ 

*Osmar Abílio de Carvalho Junior*² 

*Nickolas Castro Santana*³ 

*Roberto Arnaldo Trancoso Gomes*⁴ 

*Renato Fontes Guimarães*⁵ 

*Cristiano Rosa Silva*⁶ 

Keywords

Time series
Remote sensing
Amazon Forest
Composite image

Abstract

One challenge in the study of optical remotely sensed time series in the Amazon is the constant cloud cover. The present study evaluates different compositing techniques using regular and non-regular intervals to obtain cloud-free images over large areas. The study area was the municipality of Capixaba, State of Acre, belonging to the Amazon region. The tests considered four compositing algorithms (maximum, minimum, mean, and median) for daily MODIS sensor data (b1 and b2, 250m). The compositing technique from regular intervals adopted the following periods: 8, 16, 24, 32, 40, and 48 days. The irregular interval composite images adopted different composition intervals for dry seasons (April to September) and rainy (October to March). The cloud mask and viewing angle constraint allowed to obtain information without atmospheric interference and closest to the nadir view. The composite images using regular intervals did not allow for overcoming the high frequency of cloud cover in the region. The composite images from non-regular intervals presented a higher percentage of cloud-free pixels. The mean and median methods provided a better visual appearance of the images, corroborating with the homogeneity test. Therefore, composite images from non-regular intervals may be an appropriate alternative in places with constant cloud coverage.

¹ Instituto Federal de Brasília – IFB, Brasília, DF, Brazil. cristiane.salgado@ifb.edu.br

² Universidade de Brasília – UnB, Brasília, DF, Brazil. osmarjr@unb.br

³ Universidade de Brasília – UnB, Brasília, DF, Brazil. nickolas.santana@outlook.com

⁴ Universidade de Brasília – UnB, Brasília, DF, Brazil. robertogomes@unb.br

⁵ Universidade de Brasília – UnB, Brasília, DF, Brazil. renatofg@unb.br

⁶ Universidade de Brasília – UnB, Brasília, DF, Brazil. lincecaco@gmail.com

INTRODUCTION

One challenge in time series research using optical remote sensing in humid tropical regions is the constant cloud cover and aerosol interference (ASNER, 2001; ASNER; ALENCAR, 2010; HILKER et al., 2015). The cloud cover frequently depends on the season and the geographic position. The Amazon region has high rainfall rates (1,600 to 3,600mm annually) (FISCH et al., 1998; AB'SÁBER, 2003) with three dry months (July to September) (BI et al., 2016). During the rainy season, the cloud cover is almost constant, preventing the acquisition of images of the earth's surface (ASNER, 2001; HILKER et al., 2015). Furthermore, the difficulty persists in the dry season because of the recurrent burning events in the region that causes increased aerosol interference, despite the lower presence of clouds (SAMANTA et al., 2010; DALDEGAN et al., 2014, SANTANA et al., 2018).

Eliminating cloud and noise effects, the multitemporal compositing techniques, and the data filtering are the two main methods applied to time series. Multitemporal compositing techniques establish the best clear-sky pixels from multiple scenes over a time interval to reduce artifacts and atmospheric effects (QI; KERR, 1997). This procedure presents two main factors for analysis: the selection criteria of the best pixel and the lag time dimension.

Several selection criteria of the best pixel have been proposed such as assorting data (maximum or minimum value) (HOLBEN, 1986; CAHOON et al., 1994), statistical approach (average all cloud-free pixels) (MEYER et al., 1995; VANCUTSEM et al., 2007b), and view angle distribution (pixel closest to nadir) combined with quality flags (VAN LEEUWEN et al., 1999). One of the first methods used in the NDVI time series was the maximum value composite that adopts the highest value within each period (HOLBEN, 1986; POTTER; BROOKS, 1998). In contrast, the minimum value composite from NDVI data identified the lowest values applied in the burned area detection (CAHOON et al., 1994).

The composite image quality depends on the appropriate specification of the lag time dimension. The image compositions may be unable to detect a specific phenomenon if the length of the lag time exceeds the cycle. There is no single lag time solution for different targets and locations. Various studies assess the remote sensing responses from different lag

time dimensions, especially considering the composite MODIS products (8-day and 16-day). The 16-day has been used in phenology detection (WARDLOW et al., 2006; VINTROU et al., 2012). Thus, specific strategies of composite procedure have been developed for different environments and purposes, such as burned areas (BARBOSA et al., 1998; SOUSA et al., 2003; CHUVIECO et al., 2005; 2008; MIETTINEN; LIEW, 2008), wetland and floodplain inundation (CHEN et al., 2013), monitoring vegetation cover (ZENG et al., 2000; YANG et al., 2011) and crop mapping (XIAO et al., 2002; GUINDIN-GARCIA et al., 2012).

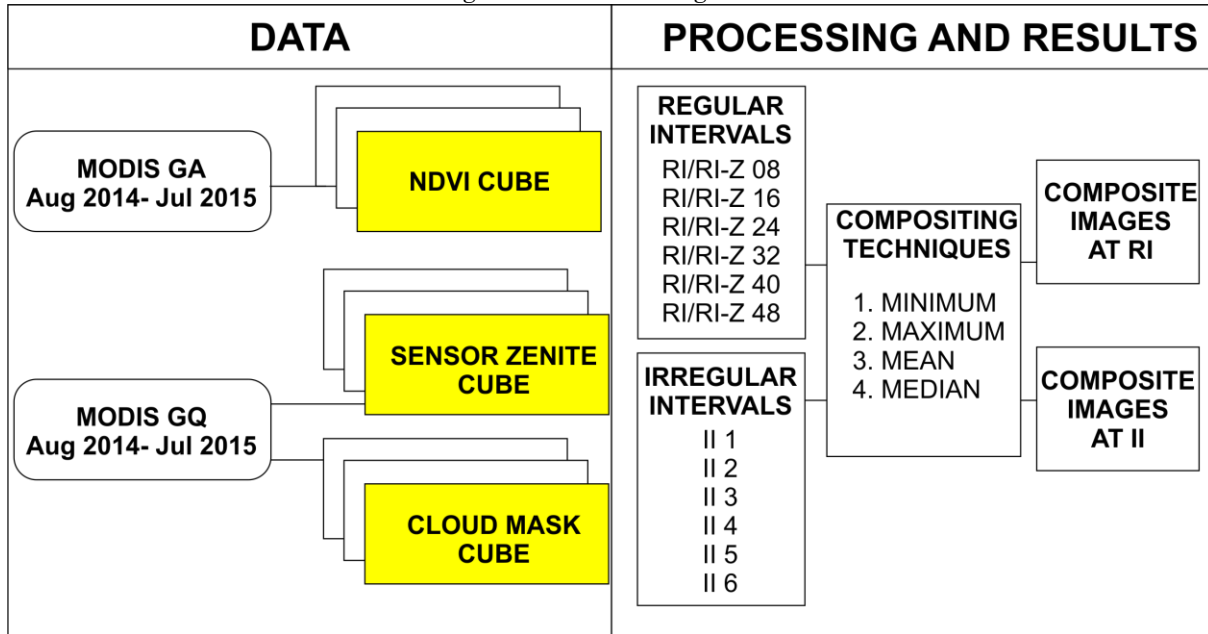
The proposed compositing methods adopt a uniformly distributed lag model. The main advantage of this distribution is to contain a detailed and continuous representation. Uniform intervals facilitate probabilistic analyses since the variation of a point and its prediction capacity are correlated with the length of the time interval. However, the complexity increases in environments with a high percentage of cloud coverage and heterogeneous distribution throughout the year. Data modeling based on uniform temporal distribution is impracticable due to the lack of data in specific periods. More flexible temporal distribution models should be studied to provide a possible representation of these locations. Nevertheless, time-series remote sensing studies have not reported alternative procedures that best exploit existing data. Data distribution with non-regular intervals requires the definition of an adaptive lag dimension from data availability, describing a time structure that best takes advantage of existing information.

While the conventional lag structure model is suitable for describing linear effects, they show some limitations when used to represent non-linear relationships. However, cloud contamination is still possible considering the localization and length of the time interval. This study aims to analyze multitemporal image compositing criteria from daily MODIS time series in the Amazon region, eliminating atmospheric interference.

MATERIALS AND METHODS

The methodological flowchart presents the various processing steps: data acquisition, NDVI calculation, composite image elaboration, and performance analysis (Figure 1).

Figure 1 - Methodological flowchart.



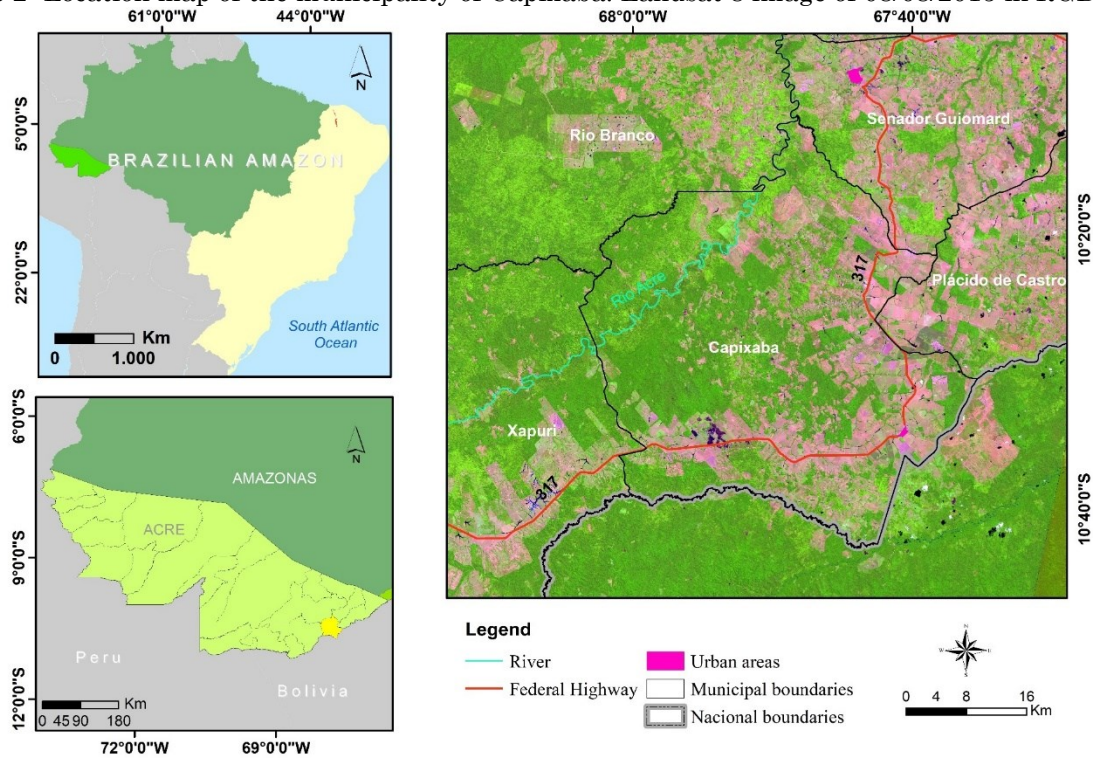
Source: The authors (2022).

Study area

The study area was the municipality of Capixaba (State of Acre) located in the Brazilian Western Amazon (Figure 2). The municipality occupies 170,257.70 hectares and it has a diversity of land use, and occupation types (land reform settlements, extractive reserves and, private property). It was the second-largest producer of sugarcane in the State (IBGE, 2016), housing a sugarcane industry for ethanol and sugar. The climatic conditions of the region establish constantly covered by clouds, possessing high relative

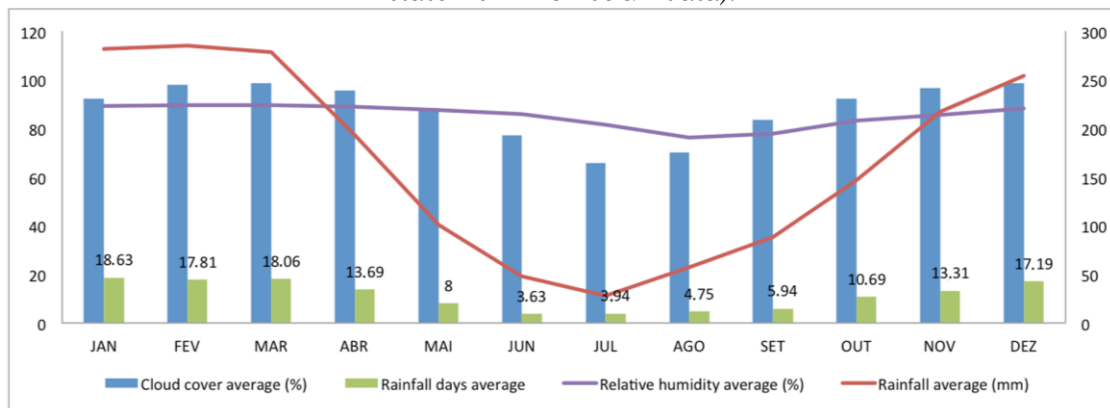
humidity (76.2 – 89.5%) throughout practically the whole year (INMET, 2015) (Figure 3). The average daily relative humidity in the rainy season is 88%, and the daily oscillation varies between 55 and 98%. During the dry period, the average is 75%, with a daily variation of 50 and 87% (DUARTE, 2006). The rainy season occurs from October to March and the wettest month is February. The dry season is from April to September and the driest month is June (FISCH et al.,1998; DUARTE, 2006). Cloud cover during the rainy season is between 7-9 days in 10 days and during drought is between 4-7 days in 10 days (DUARTE, 2006).

Figure 2- Location map of the municipality of Capixaba. Landsat 8 image of 08/08/2015 in RGB/654.



Source: The authors (2022).

Figure 3 - Climatic data for the period 2000-2015 in the State of Acre: rainfall, relative humidity, rainy days (INMET, 2022), and cloud coverage data (average for the period 2000-2015 from band state from MOD09GA data).



Source: The authors (2022).

MODIS images

The MODIS sensor has 36 spectral bands at 250-, 500- and 1000-m spatial resolutions and covers the entire planet almost daily to monitor the oceans, atmosphere, and land surface (BARNES et al., 1998; GIGLIO et al., 2016). MODIS images are available for free download by the National Aeronautics and Space Agency (NASA), containing corrections for atmospheric gases, aerosols, and cirrus clouds (JUSTICE et al., 1998).

We selected the daily images of MODIS surface reflectance (MOD09GQ), relative to bands 1 and 2 (250-m resolution), and the data quality assessment (QA-state) of the MOD09GA product (1-km resolution) during the period from August 1, 2014, to July 31, 2015. This year's choice was due to precise field control. The sinusoidal MODIS data in HDF format (over title h11v10) was converted to the GeoTIFF format, Geographic projection, and WGS84 Datum, using the MODIS Reprojection Tool software (DWYER; SCHMIDT, 2006). The daily Normalized Difference Vegetation Index

(NDVI) calculation used bands 1 (red) and 2 (near-infrared).

Unfortunately, the Reflectance Band Quality of the MOD09GQ product (250-m resolution) does not have reliable information (DAAC; FALLS, 2014). Therefore, we choose to use the State QA of the MOD09GA daily product, containing a 16-bits binary string and 11 parameters: cloud state, cloud shadow, land/waterflag, aerosol quantity, cirrus detected, internal cloud algorithm flag, internal fire algorithm flag, MOD35 snow/ice flag, pixel is adjacent to cloud, BRDF correction performed, and internal snow mask. The 1 km reflectance data State QA is in decimal numbers, requiring conversion to the binary number for the selection of pixels of interest.

We elaborate a cloud-free mask, considering the following parameters: cloud state (clear), aerosol quantity (climatology, low and average), and land/water flag (land, shallow inland water, ephemeral water, deep inland water). The 1-km spatial resolution mask was resized to 250-m to be compatible with the surface reflectance images. The Sensor Zenith Angle (SZA) from MOD09GA (1km) product detected the observation closest to the SZA

nadir, establishing specific geometry and shading conditions (BARBOSA et al., 1998; WOLFE et al., 1998; CHUVIECO et al., 2005; LI et al., 2016).

Evaluation of compositing techniques

We tested the following composite image algorithms: minimum (MIN), maximum (MAX), means (MC), and median (MDN), considering regular and irregular interval configurations. All the compositing algorithms were developed in C++ language within the Abilius software, an open-access image processing program developed by the Laboratório de Sistemas de Informações Espaciais (LSIE), a laboratory linked to the University of Brasilia and carrying out space research using modern technologies. The compositing technique from regular intervals (RI) adopted the following periods: 8, 16, 24, 32, 40, and 48 days (Table 1). The tests considered two situations: (a) only the cloud-free pixels; and (b) cloud-free pixels and SZA restriction to the interval between 0 and 40° (MIETTINEN; LIEW, 2008; VANCUTSEM; DEFOURNY, 2009).

Table 1 - Composite images with regular intervals (RI). The RI-Z models represent the results with viewing angle constraint (0 – 40°).

Model 1 (RI) (Cloud free pixels)	Model 2 (RI-Z) (Cloud-free pixels + restricted zenith sensor angle)	Regular intervals
RI-8	RI-Z-8	8 days
RI-16	RI-Z-16	16days
RI-24	RI-Z-24	24 days
RI-32	RI-Z-32	32days
RI-40	RI-Z-40	40 days
RI-48	RI-Z-48	48 days

Source: The authors (2022).

The irregular interval composite images adopted different composition intervals for dry seasons (April to September) and rainy (October to March) (Table 2). The time lag in the wet season increases due to persistent cloud cover. Meanwhile, the dry period used the

10-day range. In the II-4 and II-5 tests, the periods used for the rainy season included April and May days. The last test (II-6) adopted one image per month and at least two in the rainy season.

Table 2 - Number of days over the months used to build composite images with irregular intervals (II). For example, three composite images of 10 days make up the month of August.

	AUG 2014	SEP 2014	OCT 2014	NOV 2014	DEC 2014	JAN 2015	FEB 2015	MAR 2015	APR 2015	MAY 2015	JUN 2015	JUL 2015	Total composite images
II-1	10,10,10	10,10,10		15,15,15,15,15,15,15,15,15,15,15,15					10,10,10	10,10,10	10,10,10	10,10,10	30
II-2	10,10,10	10,10,10		30, 30, 30, 30, 30, 30					10,10,10	10,10,10	10,10,10	10,10,10	24
II-3	10,10,10	10,10,10		45,45,45,45					10,10,10	10,10,10	10,10,10	10,10,10	22
II-4	10,10,10	10,10,10		50,50,50,50					10	10,10,10	10,10,10	10,10,10	21
II-5	10,10,10	10,10,10		60,60,60,60							10,10,10	10,10,10	16
II-6	30	30		90, 90					30	30	30	30	8

Source: The authors (2022).

Comparative evaluation of multitemporal compositing techniques

The comparison among multitemporal compositing techniques used three procedures: (a) visual inspection; (b) differences between composite and reference images (CIHLAR et al., 1994); and (c) statistical analysis of heterogeneity based on the coefficient of variation (CV) (MIETTINEN; LIEW, 2008). The visual inspection sought to detect artificial heterogeneity and the presence of artifacts that did not correspond to the surface characteristics due to data acquisition errors.

The relative ranking proposed by Cihlaret al. (1994) generates an image of the subtraction between the reference and composite images and analyzes their histograms. We adapted the method to produce the image of the absolute value of the subtraction between the images, followed by the calculation of its mean. The lowest value corresponds to the best model. The reference image (June 20, 2015) selection considered two conditions: minimum cloud cover, and satellite track closest to the center of the study area (CIHLAR et al., 1994).

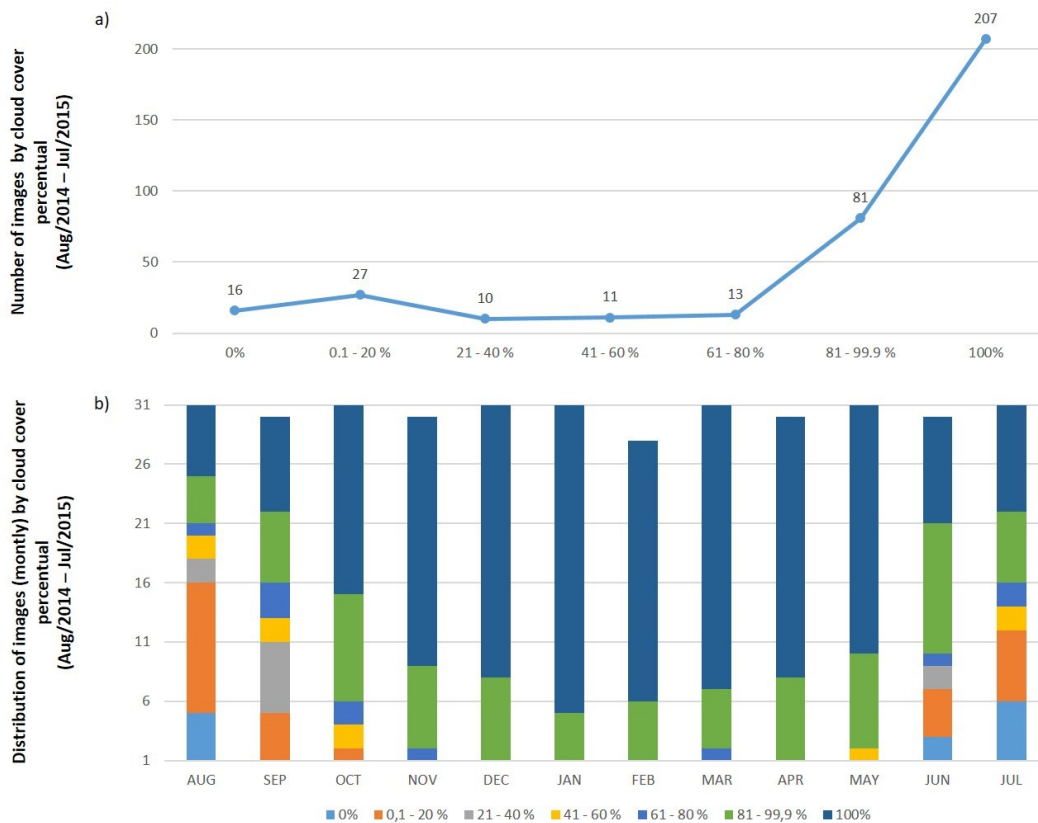
The spatial homogeneity analysis adopted the following steps (MIETTINEN; LIEW, 2008): (a) use of a 5x5 pixel moving window that calculates the CV; and (b) calculation of the mean value of this composite image filtered

by CV. The lower mean value between the methods corresponds to the more homogeneous behavior and the best technique. However, this procedure favors the MAX method because it has variations with low amplitudes and a division by the highest average. Therefore, the result may not prove the best image quality. To minimize this effect, we proposed to join the two methods by calculating the absolute of the subtraction between the CV images (reference and composite images). The homogeneity analyses considered only the 100% cloud-free pixel images for each test (RI-8, RI-16, RI-24, RI-32, RI-40, and RI-48).

RESULTS

The cloud mask time series contained 365 images (August 2014/July 2015), of which 207 images had total cloud coverage (56.7%) and 81 images (22.2%) ranging from 81 to 99.9% cloud coverage (Figure 4). Therefore, approximately 80% of the images emphasized the strong presence of clouds in the region, and the cloud-free images were poorly distributed throughout the year. Cloud cover intensified in the months of the rainy season between October and March, while the lowest cloud cover occurred in the period from June to September.

Figure 4 - Percentage cloud statistics within the time series (August 2014 to July 2015): (a) total images per percentage of cloud cover; and (b) monthly distribution of cloud cover percentage.

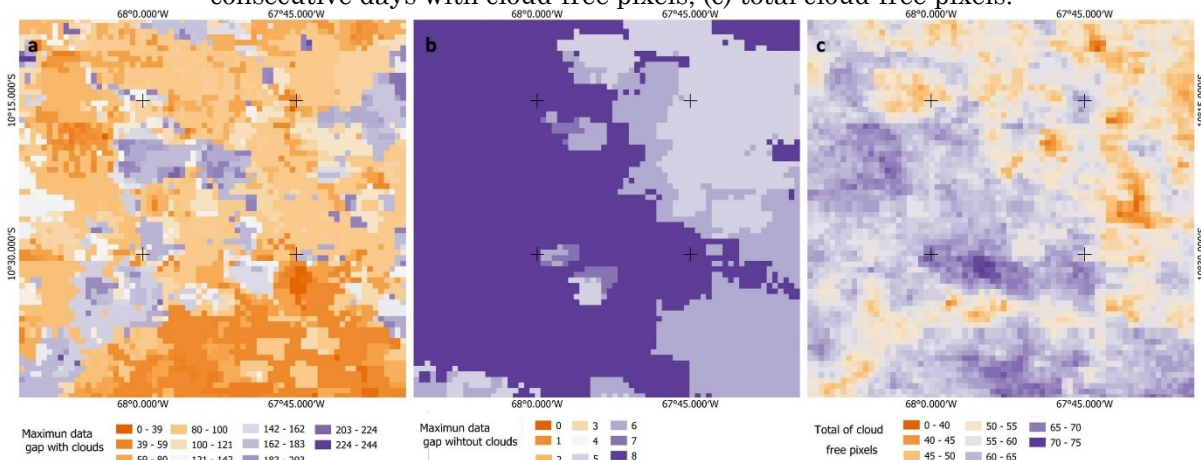


Source: The authors (2022).

In the time series analyzed, the maximum cloud cover range without interruption at one pixel was 244 days (Figure 5A). Meanwhile, the maximum cloud-free range without interruption at one pixel was eight days

(Figure 5B). The frequency of cloud coverage varies spatially (Figure 5C). The maximum number of cloud-free pixels throughout the time series was 75 (with or without interruption).

Figure 5 - Images of statistics per pixel from the daily cloud coverage mask (August 2014 to July 2015): (a) maximum range of consecutive days with cloud coverage; (b) maximum interval of consecutive days with cloud-free pixels; (c) total cloud-free pixels.



Source: The authors (2022).

Composite images with regular intervals

In the 8-day composite images (RI-8), 11 images have 100% information from a total of

45 images, representing 24.4% (Table 3). SZA restriction decreases to 7 (15.6%) images. Most of the resulting images have up to 20% of the information.

Table 3 - Distribution of the number of composite images using regular intervals (RI) by the percentage of valid observations. The Z models represent the results with viewing angle constraint (0 – 40°).

Models	Total composite images	Distribution of the number of composite images (and their respective percentage) by the percentage of pixels with valid data					
		0 - 20%	21 - 40%	41 - 60%	61 - 80%	81 - 99%	100%
RI-8	45	20 (0.44%)	6 (0.13%)	4 (0.09%)	0 (0.00%)	4 (0.09%)	11 (24.4%)
RI-Z-8		23 (0.51%)	4 (0.09%)	4 (0.09%)	1 (0.02%)	6 (0.13%)	7 (15.6%)
RI-16	22	7 (0.16%)	3 (0.07%)	3 (0.07%)	1 (0.02%)	2 (0.04%)	6 (27.3%)
RI-Z-16		10 (0.22%)	1 (0.02%)	3 (0.07%)	1 (0.02%)	2 (0.04%)	5 (22.7%)
RI-24	15	4 (0.09%)	0 (0.00%)	3 (0.07%)	1 (0.02%)	2 (0.04%)	5 (33.3%)
RI-Z-24		4 (0.09%)	2 (0.04%)	2 (0.04%)	1 (0.02%)	2(0.04%)	4 (26.7%)
RI-32	11	1 (0.02%)	3 (0.07%)	1 (0.02%)	0 (0.00%)	2 (0.04%)	4 (36.4%)
RI-Z-32		3 (0.07%)	1 (0.02%)	2 (0.04%)	1 (0.02%)	1 (0.02%)	3(27.3%)
RI-40	9	0 (0.00%)	1 (0.02%)	3 (0.07%)	0 (0.00%)	2 (0.04%)	3(33.3%)
RI-Z-40		1 (0.02%)	1 (0.02%)	2 (0.04%)	0 (0.00%)	3 0.07	2(22.2%)
RI-48	7	0 (0.00%)	1 (0.02%)	2 (0.04%)	0 (0.00%)	1 (0.02%)	3(42.9%)
RI-Z-48		1 (0.02%)	1 (0.02%)	1 (0.02%)	1 (0.02%)	1 (0.02%)	2(28.6%)

Source: The authors (2022).

The RI-16 model resulted in 22 images of which only 6 (27.3%) had 100% of the information. The RI-24 and RI-32 tests resulted in 5(33.3%) and 4(36.4%) cloudless images. The RI-40 and RI-48 models resulted in only 3 images with 100% valid observations. The RI-48 test produced the highest proportion of images with valid observations, with 42.9% of

the total. Tests with viewing angle constraint (RI-Z) presented fewer images with 100% valid observations in all periods. The RI-Z-8 test showed the highest proportion of cloudless images (2 of 7 images). Both tests (RI- and RI-Z) obtained images with a percentage of 80 to 99% of cloudless pixels (Figure 6).

Figure 6 - Comparison between compositions with regular intervals (with and without the use of zenith sensor angle restriction) considering the percentage of valid pixels in the composition.



Source: The authors (2022).

The highest percentage of free pixels occurred in the driest months (August/September 2014 and June/July 2015), which provides good composite images with shorter time intervals. The first image (August/2014), for example, had 55.9% of valid observations in 4 images, 37% in 5 images, and 7.1% in 3 images. In the rainy months, the few observations found are in only 1 or 2 scenes. In some periods, there was no valid observation.

In the comparison among the compositing techniques, the analysis using the difference between the composite and the reference image obtained complete supremacy of the MDN method that reached the lowest values in all the simulations (Table 5). The second-best performance was MC for all simulations using RI and RI-Z data.

Table 5 - Averages of subtraction between reference and composition images from regular intervals (RI) or with viewing angle restriction between 0 and 40° (RI-Z).

TEST	MAX	MIN	MC	MDN
RI-8	10.76	1.64	3.33	1.50
RI-16	11.05	3.82	2.28	1.33
RI-24	11.07	4.28	2.29	1.35
RI-32	11.62	6.79	2.03	1.49
RI-40	11.82	9.09	9.09	1.64
RI-48	11.15	6.33	2.12	1.41
Average RI	11.24 (4)	5.32(3)	3.52(2)	1.45 (1)
RZ-8	0.85	1.19	0.94	0.85
RZ-16	2.45	2.98	1.20	0.91
RZ-24	2.91	3.44	1.26	0.92
RZ-32	2.69	5.26	1.55	1.23
RZ-40	2.73	7.46	2.18	1.70
RZ-48	3.65	5.11	1.42	1.01
Average RIZ	2.55 (3)	4.24(4)	1.43(2)	1.10(1)

Source: The authors (2022).

As expected, the heterogeneity analysis demonstrated that the MAX method obtained the lowest CV for all the simulations (Table 6).

However, visual inspection demonstrated that the lower CV does not necessarily express improvement in image quality.

Table 6 - Average homogeny values considering composite images at regular intervals without and with reference subtraction.

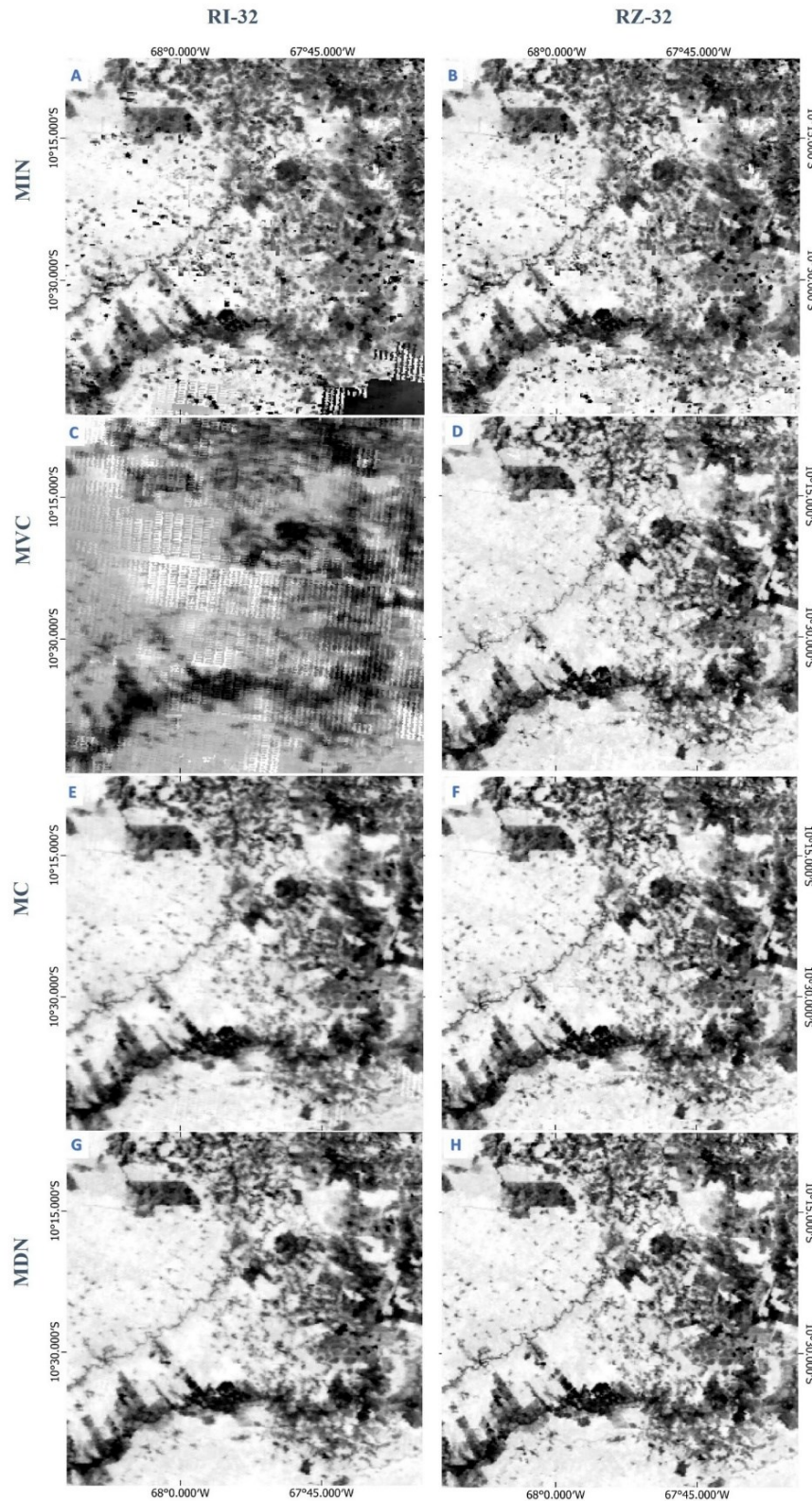
TEST	Normal				reference subtraction			
	MAX	MIN	MC	MDN	MAX	MIN	MC	MDN
RI-8	3.52	5.97	3.99	4.08	1.97	0.82	1.41	1.18
RI-16	3.31	6.90	3.88	4.00	2.06	2.21	1.19	1.00
RI-24	3.19	7.40	3.80	3.88	1.85	4.00	1.25	1.22
RI-32	3.17	8.31	3.88	3.95	2.19	4.27	1.21	1.11
RI-40	2.99	9.31	3.80	3.92	2.17	4.84	1.13	1.08
RI-48	2.95	9.54	3.79	3.91	2.09	5.22	1.18	0.96
Average RI	3.19	7.91	3.86	3.96	2.05	3.56	1.23	1.09
RI-Z-8	4.79	5.78	5.05	5.08	0.62	0.56	0.51	0.49
RI-Z-16	4.75	6.71	5.16	5.14	0.88	1.41	0.54	0.44
RI-Z-24	4.49	7.28	5.02	5.04	1.08	3.55	1.46	1.43
RI-Z-32	4.21	8.05	4.98	4.98	0.95	2.93	0.63	0.52
RI-Z-40	3.96	8.01	4.77	4.79	0.98	3.86	0.77	0.65
RI-Z-48	3.93	8.65	4.63	4.57	1.17	4.22	0.74	0.50
Average RIZ	4.36	7.41	4.94	4.93	0.94	2.75	0.77	0.67

Source: The authors (2022).

The MAX image presented noisy artifacts and eliminated important natural features like river lines (Figure7). Therefore, high, or low CV values may represent quality loss and should be calibrated by reference value. As in the

direct subtraction between the reference and composite images, the results of the diminution of the CV images also showed superior results for the MDN method.

Figure 7 - First 32-day composite image for the 4 methods (MIN, MAX, MC, MDN), considering L32 (A, C, E, G) and LZ32 (B, D, F, H) tests.



Source: The authors (2022).

These results corresponded to the visual inspection, with the MDN and MC methods resulted in more homogeneity (Figures 7 E, G). Meanwhile, the MIN and MAX methods

resulting in more heterogeneous composite images containing the presence of atmospheric and noisy effects. (Figures 7A, C). The SZA restriction resulted in more homogeneous

images according to the methods of subtraction and visual inspection (Tables 5 and 6).

Composite images with irregular intervals

The tests with irregular intervals of II-1 to II-5 sought to maintain the same range for the dry period (10 days) and varied the rainy period

(15, 30, 45, 50, and 60 days), the last test (II-6) changed the dry period values to 30 days (Table 2).

In test II-1, 8 of the 12 composite images in the rainy season had <50% accurate observations, 2 reaches 50%, and 2 around 100% during September and October (Table 7).

Table 7 - Distribution of quantitative images by the percentage of valid information.

Composite	Number of images per percentage of information						Total	Percentage of observations 100% valid in the test
	0 - 20%	21 - 40%	41 - 60%	61 - 80%	81 - 99%	100%		
II-1	9	3	5	0	4	9	30	30.0
II-2	6	1	4	1	3	9	24	37.5
II-3	5	1	3	1	2	9	21	42.9
II-4	3	1	4	0	3	9	20	45.0
II-5	0	1	2	1	3	9	16	56.3
II-6	0	1	0	1	1	5	8	62.5

Source: The authors (2022).

In contrast, 8 of the 18 composite images in the dry period presented 100% correct information. However, some composite images

of the dry season did not reach 50% of valid observations (Table 8).

Table 8 - Percentage of cloudless image quantity used in composite images of the test II-1 (%).

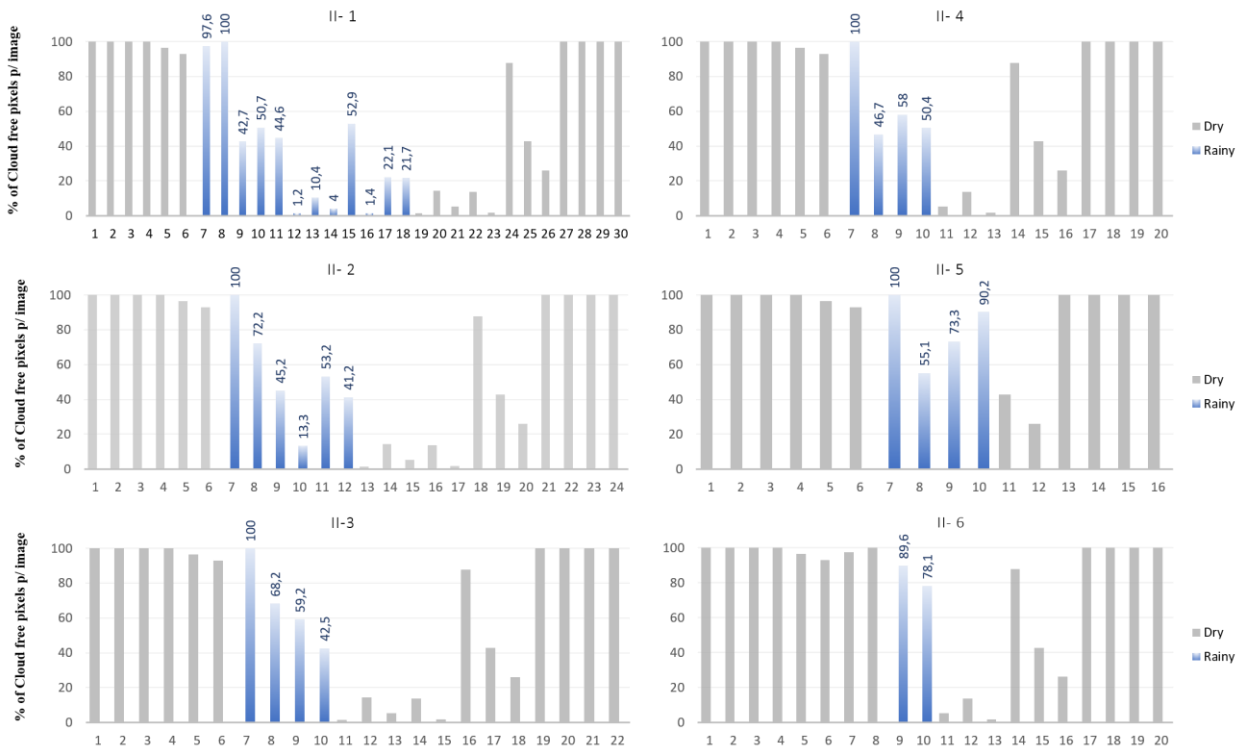
Composite images	Number of cloud-free images used in the 8-day composite image											Sum
	1	2	3	4	5	6	7	8	9	10	>10	
Img 1/Aug	0	0	0	5	53.3	38.4	3.3	0	0	0	0	100
Img 2/Aug	0	0	0	0	1.1	40.4	56.4	2.1	0	0	0	100
Img 3/Aug	0	1.1	7	19.3	22.1	28.7	18.8	3.1	0	0	0	100
Img 4/Sep	0	0.4	1.2	7.2	16.2	40.8	28.8	5.4	0	0	0	100
Img 5/Sep	17.2	25.2	28.3	19	6.6	0.1	0	0	0	0	0	96.4
Img 6/Sep	22.8	25.7	35.6	7	1.9	0	0	0	0	0	0	92.9
Img 7/Oct	32.6	30.2	26.9	7.6	0.3	0	0	0	0	0	0	97.6
Img 8 /Oct	0.3	51.6	48	0.1	0	0	0	0	0	0	0	100
Img 9/ Nov	38	4.6	0	0	0	0	0	0	0	0	0	42.7
Img 10/Nov	42.2	8.5	0	0	0	0	0	0	0	0	0	50.7
Img 11/Dec	41	3.7	0	0	0	0	0	0	0	0	0	44.6
Img 12/Dec	1.2	0	0	0	0	0	0	0	0	0	0	1.2
Img 13/Jan	9.8	0.6	0	0	0	0	0	0	0	0	0	10.4
Img 14/Jan	4	0	0	0	0	0	0	0	0	0	0	4
Img 15/Feb	51.4	1.4	0	0	0	0	0	0	0	0	0	52.9
Img 16/Feb	1.4	0	0	0	0	0	0	0	0	0	0	1.4
Img 17/Mar	19.9	2.2	0	0	0	0	0	0	0	0	0	22.1
Img 18/Mar	21.7	0	0	0	0	0	0	0	0	0	0	21.7
Img 19/Apr	1.1	0.1	0	0	0	0	0	0	0	0	0	1.2
Img 20/Apr	14	0.1	0	0	0	0	0	0	0	0	0	14.2
Img 21/Apr	5.3	0	0	0	0	0	0	0	0	0	0	5.3
Img 22/May	13.7	0	0	0	0	0	0	0	0	0	0	13.7
Img 23/May	1.7	0	0	0	0	0	0	0	0	0	0	1.7
Img 24/May	51.8	32.6	3.3	0	0	0	0	0	0	0	0	87.7
Img 25/Jun	37.7	4.9	0.2	0	0	0	0	0	0	0	0	42.8
Img 26/Jun	19.9	5.8	0.3	0	0	0	0	0	0	0	0	26.1
Img 27/Jun	0	0	0	0.8	10.2	26.3	60.1	2.5	0	0	0	100
Img 28/Jul	0	1	15.3	60.8	19.9	3	0	0	0	0	0	100
Img 29/Jul	4.8	40.8	43.1	10.2	1.1	0	0	0	0	0	0	100
Img 30/Jul	0	0	0	0.5	26.4	63.1	9.9	0	0	0	0	100

Source: The authors (2022).

The persistence of cloud cover occurred in the first months of the dry season (mainly in April), while images with 100% valid

observations happened in the transition between dry and rainy seasons (October) (Figure 8).

Figure 8 - Results of composite images with irregular intervals considering the percentage of valid observations in each composition.



Source: The authors (2022).

The test II-6 at intervals of 90 days for the rainy season and 30 days for the dry season presented the first composite image of the rainy season with 100% of valid observations and the second with 78.1% (Figure 8). However, the third composite image presented only 18.8% of valid observations, evidencing that April and May concentrate significant cloud cover. In all the tests there were images with proportions of information between 81 and 99.9%, representing the possibility for use.

The comparison of the compositing methods demonstrated that the II tests obtained the same results as the RI tests. The method MDN and the use of SZ constraint received superior results in the procedures of subtraction and visual inspection.

DISCUSSION

The study area presents a severe restriction of valid observations during the year, containing pixels with 244 days without visibility of the earth's surface. Thus, the viable alternative is the long-term composite images with a period of at least 30 days (MIETTINEN; LIEW, 2008; VANCUTSEM; DEFOURNY, 2009). In simulations with regular intervals, most

composite images in the rainy season reach less than 50% of cloud-free pixels. Increasing the time interval did not guarantee the increase of this percentage for all composite images in the rainy season. Thus, the use of multitemporal compositing techniques at regular intervals significantly reduces the amount of data throughout the year since the rainy period controls the lag time extension. Our proposed solution to this problem is the use of composite images with irregular intervals between wet and dry periods, obtaining a greater quantity and quality of images during the year. Therefore, the customized approach becomes necessary to find a balance and a consistency of spatial and temporal data in areas with high cloud cover. Both composite images with regular and irregular intervals had 80% to 99.9% of valid observations, being suitable for land use/land cover studies since images with up to 30% cloud cover are adequate for this purpose (ASNER, 2001).

According to other research, an essential factor for the quality of composite images is the restriction of the angle of the zenith sensor (CHUVIECO et al., 2005; VANCUTSEM et al., 2007b). Therefore, the combination of the multitemporal compositing technique and the selection of pixels with quality control produces images with greater spatial consistency and

better reflectance and texture distributions, resulting in a better visual aspect (VANCUTSEM et al., 2007a; 2007b). Despite the improvement in image quality, this criterion further reduces the amount of available data. Thus, its application can be restricted to drought months, where there is a higher intensity of valid observations.

Homogeneity analysis using only the CV data did not adequately represent the image quality. Comparison with reference data demonstrated results consistent with the visual inspection. Statistical metrics of central values presented images of better quality and greater spatial consistency, and this result is evidenced by other research (e.g., VANCUTSEM et al., 2007b). In general, the selection of extreme values (minimum or maximum) favors specific studies, for example, burned area detection (SOUSA et al., 2003; CHUVIECO et al., 2005). The combination of pixel quality control plus the zenith angle restriction brought better image quality widely described in the literature (MIETTINEN; LEW, 2008).

FINAL CONSIDERATIONS

The present study evaluated compositing algorithms for MODIS data in the Amazon region considering the following factors: angular effects and atmospheric conditions; statistical procedure to establish the composite value and temporal interval. Despite reducing the number of data available, the selection of cloudless pixels and with sensor zenith angle between 0 and 40° allowed to acquire of homogenized images with a reduction of artifacts and atmospheric effects. Among the statistical methods, the median value presented the best results. The composite images using regular intervals did not allow for overcoming the high frequency of cloud cover in the region. Under these conditions, we proposed the use of irregular intervals alternatively for the composite images, adjusting the data availability. This method was more efficient in providing more data, especially in the rainy season. Customizing the composite image period allows users greater flexibility to overcome the high cloud cover for long periods.

ACKNOWLEDGMENTS

The authors are grateful the Department of Geography of the Universidade de Brasília and Instituto Federal de Brasília (IFB) for logistical support.

REFERENCES

- AB'SÁBER, A. **Os domínios de natureza no Brasil: potencialidades paisagísticas**. [The domains of nature in Brazil: landscape potential] 12th ed. São Paulo: Ateliê Editorial, 2003.
- ASNER, G. P. 2001. Cloud cover in Landsat observations of the Brazilian Amazon. **International Journal of Remote Sensing**, v. 22, p. 3855–3862, 2001. <https://doi.org/10.1080/01431160010006926>
- ASNER, G. P.; ALENCAR, A. Drought impacts on the Amazon Forest: the remote sensing perspective, **New Phytologist**, v.187, p. 569–578, 2010. <https://doi.org/10.1111/j.1469-8137.2010.03310.x>
- BARBOSA, P. M.; PEREIRA, J. M. C.; GRÉGOIRE, J. -M. Compositing Criteria for burned area assessment using multitemporal low resolution satellite data. **Remote Sensing of Environment**, v. 65, p. 38–49, 1998. [https://doi.org/10.1016/S0034-4257\(98\)00016-9](https://doi.org/10.1016/S0034-4257(98)00016-9)
- BARNES, W. L.; PAGANO, T. S.; SALOMONSON, V. V. Prelaunch characteristics of the Moderate Resolution Imaging Spectroradiometer (MODIS) on EOS-AM1. **IEEE Transactions on Geoscience and Remote Sensing**, v. 36, p. 1088–1100, 1998. <https://doi.org/10.1109/36.700993>
- BI, J. et al. Amazon Forests' response to droughts: a perspective from the MAIAC product. **Remote Sensing**, v. 8, p. 356, 2016. <https://doi.org/10.3390/rs8040356>
- CAHOON, D. R. et al. Satellite analysis of the severe 1987 forest fires in northern China and southeastern Siberia. **Journal of Geophysical Research: Atmospheres**, v. 99, p. 18,627–18,638, 1994. <https://doi.org/10.1029/94JD01024>
- CHEN, Y. et al. An evaluation of MODIS daily and 8-day composite products for floodplain and wetland inundation mapping. **Wetlands**, v. 33, p. 823–835, 2013. <https://doi.org/10.1007/s13157-013-0439-4>
- CHUVIECO, E. et al. Assessment of multitemporal compositing techniques of

- MODIS and AVHRR images for burned land mapping. **Remote Sensing of Environment**, v. 94, p. 450–462, 2005. <https://doi.org/10.1016/j.rse.2004.11.006>
- CHUVIECO, E. et al. Global burned-land estimation in Latin America using MODIS composite data. **Ecological Applications**, v. 18, p. 64–79, 2008. <https://doi.org/10.1890/06-2148.1>
- CIHLAR, J.; MANAK, D.; D'LORIO, M. Evaluation of compositing algorithms for AVHRR data over land. **IEEE Transactions on Geoscience and Remote Sensing**, v. 32, p. 427–437, 1994. <https://doi.org/10.1109/36.295057>
- DAAC, N. L. P.; FALLS, S. **MODIS Land products quality assurance tutorial: Part-1**. Sioux Falls (SD): USGS EROS Center, p. 1–17, 2014.
- DALDEGAN, G. A. et al. Spatial patterns of fire recurrence using remote sensing and GIS in the Brazilian Savanna: Serra do Tombador Nature Reserve, Brazil. **Remote Sensing**, v. 6, p. 9873–9894, 2014. <https://doi.org/10.3390/rs6109873>
- DUARTE, A. F. 2006. Aspectos da climatologia do Acre, Brasil, com base no intervalo 1971-2000 [Aspects of the climatology of Acre, Brazil, based on the interval 1971-2000]. **Revista Brasileira de Meteorologia**, v. 21, p. 308–317, 2006.
- DWYER, J.; SCHMIDT, G. 2006. The MODIS Reprojection Tool. In: Qu, J. J. et al. (Editors). **Earth sciencesatelliteremotesensing**. Berlin: Springer, 2006. p. 162–177. https://doi.org/10.1007/978-3-540-37294-3_9
- FISCH, G.; MARENGO, J. A.; NOBRE, C. A. Uma revisão geral sobre o clima da Amazônia. [A general review on the climate of the Amazon]. *Acta Amazônica*, v. 28, p. 101–126, 1998. <https://doi.org/10.1590/1809-43921998282126>
- GIGLIO, L.; SCHROEDER, W.; JUSTICE, C. O. The collection 6 MODIS active fire detection algorithm and fire products. **Remote Sensing of Environment**, v. 178, p. 31–41, 2016. <https://doi.org/10.1016/j.rse.2016.02.054>
- GUINDIN-GARCIA, N. et al. An evaluation of MODIS 8- and 16-day composite products for monitoring maize green leaf area index. **Agricultural and Forest Meteorology**, v. 161, p. 15–25, 2012. <https://doi.org/10.1016/j.agrformet.2012.03.012>
- HILKER, T. et al. On the measurability of change in Amazon vegetation from MODIS. **Remote Sensing of Environment**, v. 166, p. 233–242, 2015. <https://doi.org/10.1016/j.rse.2015.05.020>
- HOLBEN, B. N. Characteristics of maximum-value composite images from temporal AVHRR data. **International Journal of Remote Sensing**, v. 7, p. 1417–1434, 1986. <https://doi.org/10.1080/01431168608948945>
- IBGE - Instituto Brasileiro de Geografia e Estatística (BR). **Pesquisa de informações básicas municipais - cidades**. [Search by basic municipal sources - cities]. 2016. Available: <https://cidades.ibge.gov.br/>. Accessed on: Dec 15, 2018.
- INMET - Instituto Nacional de Meteorologia. **BDMEP - Banco de Dados Meteorológicos para Ensino e Pesquisa**. [Meteorological Database for Teaching and Research]. 2015. Available: <http://www.inmet.gov.br/>. Accessed on: Dec 15, 2018.
- JUSTICE, C. O. et al. The Moderate Resolution Imaging Spectroradiometer (MODIS): land remote sensing for global change research. **IEEE Transactions on Geoscience and Remote Sensing**, v. 36, p. 1228–1249, 1998. <https://doi.org/10.1109/36.701075>
- LI, H.; LI, X.; XIAO, P. Impact of sensor zenith angle on MOD10A1 data reliability and modification of snow cover data for the Tarim River Basin. **Remote Sensing**, v. 8, p. 1–18, 2016. <https://doi.org/10.3390/rs8090750>
- MEYER, D.; VERSTRAETE, M.; PINTY, B. The effect of surface anisotropy and viewing geometry on the estimation of NDVI from AVHRR. **Remote Sensing Reviews**, v. 12, p. 37–41, 1995. <https://doi.org/10.1080/02757259509532272>
- MIETTINEN, J.; LIEW, S. C. Comparison of multitemporal compositing methods for burnt area detection in Southeast Asian conditions. **International Journal of Remote Sensing**, v. 29, p. 1075–1092, 2008. <https://doi.org/10.1080/01431160701281031>
- POTTER, C. S.; BROOKS, V. Global analysis of empirical relations between annual climate and seasonality of NDVI. **International Journal of Remote Sensing**, v. 19, p. 2921–2948, 1998. <https://doi.org/10.1080/014311698214352>
- QI, J.; KERR, Y. On current compositing algorithms. **Remote Sensing Reviews**, v. 15, p. 235–256, 1997. <https://doi.org/10.1080/02757259709532340>
- SAMANTA, A. et al. Amazon forests did not green-up during the 2005 drought. **Geophysical Research Letters**, v. 37, p. 1–5, 2010. <https://doi.org/10.1029/2009GL042154>

- SANTANA, N. C. et al. Burned-area detection in amazonian environments using standardized time series per pixel in MODIS data. **Remote Sensing**, v. 10, p. 1904, 2018. <https://doi.org/10.3390/rs10121904>
- SOUSA, A. M. O.; PEREIRA, J. M. C.; SILVA, J. M. N. Evaluating the performance of multitemporal image compositing algorithms for burned area analysis. **International Journal of Remote Sensing**, v. 24, p. 1219–1236, 2003. <https://doi.org/10.1080/01431160110114466>
- VAN LEEUWEN, W. J. D.; HUETE, A. R.; LAING, T. W. MODIS vegetation index compositing approach: A prototype with AVHRR data. **Remote Sensing of Environment**, v. 69, p. 264–280, 1999. [https://doi.org/10.1016/S0034-4257\(99\)00022-X](https://doi.org/10.1016/S0034-4257(99)00022-X)
- VANCUTSEM, C. et al. An assessment of three candidate compositing methods for global MERIS time series. **Canadian Journal of Remote Sensing**, v. 33, p. 492–502, 2007a. <https://doi.org/10.5589/m07-056>
- VANCUTSEM, C. et al. Mean Compositing, an alternative strategy for producing temporal syntheses. Concepts and performance assessment for SPOT VEGETATION time series. **International Journal of Remote Sensing**, v. 28, p. 5123–5141, 2007b. <https://doi.org/10.1080/01431160701253212>
- VANCUTSEM, C.; DEFOURNY, P. A decision support tool for the optimization of compositing parameters. **International Journal of Remote Sensing**, v. 30, p. 41–56, 2009. <https://doi.org/10.1080/01431160802036375>
- VINTROU, E. et al. Mapping fragmented agricultural systems in the Sudano-Sahelian environments of Africa using random forest and ensemble metrics of coarse resolution MODIS imagery. **Photogrammetric Engineering and Remote Sensing**, v. 78, p. 839–848, 2012. <https://doi.org/10.14358/PERS.78.8.839>
- WARDLOW, B. D.; KASTENS, J. H.; EGBERT, S. L. Using USDA crop progress data for the evaluation of green up onset date calculated from MODIS 250-meter data. **Photogrammetric Engineering & Remote Sensing**, v. 72, p. 1225–1234, 2006. <https://doi.org/10.14358/PERS.72.11.1225>
- WOLFE, R. E.; ROY, D. P.; VERMOTE, E. MODIS land data storage, gridding, and compositing methodology: Level 2 grid. **IEEE Transactions on Geoscience and Remote Sensing**, v. 36, p. 1324–1338, 1998. <https://doi.org/10.1109/36.701082>
- XIAO, X. et al. Landscape-scale characterization of cropland in China using vegetation and Landsat TM images. **International Journal of Remote Sensing**, v. 23, p. 3579–3594, 2002. <https://doi.org/10.1080/01431160110106069>
- YANG, Z. et al. Vegetation condition indices for crop vegetation condition monitoring. Proceedings of the IEEE International Geoscience and Remote Sensing Symposium; Jul 24-29; Vancouver, BC, Canada. IEEE, p. 3534–3537, 2011. <https://doi.org/10.1109/IGARSS.2011.6049984>
- ZENG, X. et al. Derivation and evaluation of global 1-km fractional vegetation cover data for land modeling. **Journal of Applied Meteorology and Climatology**, v. 39, p. 826–839, 2000. [https://doi.org/10.1175/1520-0450\(2000\)039<0826:DAEOGK>2.0.CO;2](https://doi.org/10.1175/1520-0450(2000)039<0826:DAEOGK>2.0.CO;2)

AUTHORS' CONTRIBUTION

Cristiane Batista Salgado and Osmar Abílio de Carvalho Junior conceptualized, curated the data, made the formal analysis, investigated, carried out the methodology, visualized, wrote – original draft, reviewed and edited. Furthermore, Osmar Abílio de Carvalho Junior worked with the software. Nickolas Castro Santana curated the data, made the formal analysis and investigated. Roberto Arnaldo Trancoso Gomes conceptualized, curated the data, made the formal analysis, investigated, carried out the methodology. Renato Fontes Guimarães curated the data, made the formal analysis, investigated and carried out the methodology. Cristiano Rosa Silva carried out the methodology and the Software.



This is an Open Access article distributed under the terms of the Creative Commons Attribution License, which permits unrestricted use, distribution, and reproduction in any medium, provided the original work is properly cited